Socio-Economic Planning Sciences 46 (2012) 33–45

Contents lists available at ScienceDirect

Socio-Economic Planning Sciences

journal homepage: www.elsevier.com/locate/seps

Dynamic redistribution of mitigation resources during influenza pandemics

Alex Savachkin*, Andrés Uribe

Department of Industrial & Management Systems Engineering, University of South Florida, 4202 E. Fowler Ave., ENB118, Tampa, FL 33620, USA

ARTICLE INFO

Article history:
Available online 12 June 2011

Keywords:
Influenza pandemic
Mitigation
Resources
Dynamic
Redistribution

ABSTRACT

The Institute of Medicine (IOM) has pointed out that the existing pandemic mitigation models lack the dynamic decision support capability. In this paper, we present a simulation optimization model to generate dynamic strategies for distribution of limited mitigation resources, such as vaccines and antivirals, over a network of regional outbreaks. The model has the capability to redistribute the resources remaining from previous allocations in response to changes in the pandemic progress. The model strives to minimize the impact of ongoing outbreaks and the expected impact of potential outbreaks, considering measures of morbidity, mortality, and social distancing, translated into the societal and economic costs of lost productivity and medical services. The model is implemented on a simulated H5N1 outbreak involving four counties in the state of Florida, U.S. with over four million inhabitants. The performance of our strategy is compared to that of a myopic distribution strategy. Sensitivity analysis is performed to assess the impact of variability of some critical factors on policy performance. The methodology is intended to support public health policy on effective distribution of limited mitigation resources.

1. Introduction

As of October 2010, the World Health Organization (WHO) has reported 505 confirmed human cases of avian influenza A/(H5N1), which resulted in 300 deaths [1]. At the same time, worldwide more than 214 countries and overseas territories have reported laboratory confirmed cases of pandemic influenza (PI) H1N1 2009, including over 18,449 deaths. [2]. Because of a continuous reassortment and mutation of the influenza virus, an ominous expectation exists today that the next pandemic will be triggered by a highly pathogenic strain to which there is little or no pre-existing immunity in humans [3–5]. A study by the Congressional Budget Office estimates that the consequences of a severe pandemic could, in the U.S. alone, include 200 million people infected, 90 million clinically ill, and 2 million dead [6]. The study estimates that 30 percent of all workers would become ill and 2.5 percent would die, with 30 percent of workers missing a mean of three weeks of work. Furthermore, 18 million to 45 million people would require outpatient care, and economic costs would total approximately $675 billion.

The nation's ability to mitigate a pandemic influenza depends on the available emergency response resources and infrastructure, and at present, challenges abound. Predicting the exact virus subtype remains a difficult task, and even when identified, a surge production of an adequate vaccine supply can currently take up to nine months [7,8]. Even if the existing vaccines prove to be potent, their availability will be limited by high production and inventory costs [9,10]. Also will be constrained the supply of antiviral agents, healthcare providers, hospital beds, medical supplies, personal protective equipment, and logistics [11–13]. Hence, pandemic mitigation will have to be done amidst limited availability of resources and supporting infrastructure. The pressing need for strategies aimed at efficient distribution of limited resources has been acknowledged by WHO [10] and echoed by the U.S. Department of Health and Human Services (HHS) and the Centers for Disease Control and Prevention (CDC) [14,15].

2. Current literature

The existing models on PI containment and mitigation can broadly be classified into: (i) statistical, (ii) mathematical, (iii) simulation-based, and (iv) combinations of thereof. In what follows, we present a summary survey of these approaches mostly focusing on simulation-based models.

The statistical models driven mainly by likelihood and regression-based approaches have primarily been used for assessment of epidemiological parameters and estimation of pandemic impact [16–18]. These models have inherently featured relatively simple and general spatio-temporal structures, such as homogeneous mixing groups, where individuals are assumed to have the same attributes [19–22].

* Corresponding author. Tel.: +1 813 974 5577.
E-mail address: alexs@usf.edu (A. Savachkin).

0038-0121/$ – see front matter © 2011 Elsevier Ltd. All rights reserved.
doi:10.1016/j.seps.2011.05.001

The mathematical models have mostly focused on modeling virus spread and policy assessment. Notable examples of such models are dynamic compartmental approaches, typically represented in the form of a set of differential equations, which delineate transitions between disease phases (e.g., susceptible, exposed, symptomatic infected, etc.) [23–26]. Based on the solution approach, the mathematical models can be subdivided into analytical (or closed form) and iterative. Compared to the statistical models, the dynamic-iterative models feature more granular composition of the mixing groups [23–28]. However, the degree of granularity is still limited since any additional spatio-temporal considerations can negatively impact the computational robustness of the models. Description of the contact processes in mathematical models generally does not take into account changes in the behavioral patterns during the course of the pandemic (e.g., compliance to intervention by vaccination and social distancing) [24–26]. Such considerations can be found in some of the recent simulation-based models [29–32]. Furthermore, mathematical models are typically based on the infection pathways and disease progression that are invariant to time and individual attributes [25,26].

The simulation-based approaches have been used for modeling virus spread and assessment and generation of pharmaceutical and/or non-pharmaceutical interventions. Based on the way of generating disease progression, these models can be categorized as those that track infection pathway of each individual entity [33–39] and the rest that are driven by occurrence of infection events [40,41]. In contrast to the statistical and mathematical models, the simulation models are capable of providing most detailed description of population dynamics whereby each individual can be assigned a set of attributes (e.g., age, gender, community, etc), that can be modified without altering the general model structure [35,42]. However, such comprehensive descriptive granularity is achieved at the expense of higher data demand and more substantial computational burden. As a result, most existing simulation-based approaches incorporate statistical and/or mathematical submodels (e.g., for infection generation) in order to attain an effective balance between model accuracy and practicality [35,39].

The recent simulation-based models aim to address various complex aspects of the pandemic evolution process including: (i) the mechanism of disease progression, from the initial contact and infection transmission, to the asymptomatic phase, manifestation of symptoms, and the final health outcome [43–45], (ii) the population dynamics, including individual susceptibility [46,47] and transmissibility [16,19,43,48], and behavioral factors affecting infection generation and effectiveness of interventions [49–51], (iii) the impact of pharmaceutical and non-pharmaceutical measures, including vaccination [20,22,52], antiviral therapy [26,53,54], social distancing [29–32,55] and travel restrictions, and the use of low-cost measures, such as face masks and hand washing [27,41,54,56].

Most recently, the modeling efforts have focused on combining pharmaceutical and non-pharmaceutical interventions in search for synergistic strategies aimed at better resource utilization. Significant contributions in this area include [33,38,40,41,57–60]. One of the most notable among these efforts is a 2006–2007 initiative by MIDAS [61], which cross-examined independent simulation models of PI spread in rural areas of Asia [36,62], U.S. and U.K. [34,37], and the city of Chicago [63], respectively. MIDAS cross-validated the models by simulating the city of Chicago, with 8.6 M inhabitants, and implementing a targeted layered containment [64,65]. The research findings of MIDAS and some other groups [41,45] were used in a recent "Modeling Community Containment for Pandemic Influenza" report by IOM, to formulate a set of recommendations for PI mitigation [66]. These findings were also used in a pandemic preparedness guidance developed by CDC [67].

The IOM report [66] points out several *limitations* of the MIDAS models, observing that "because of the significant constraints placed on the models… the scope of models should be expanded." IOM recommends "to develop *decision-aid models* that can… provide *real-time feedback*… and include the *costs and benefits* of intervention strategies". Our literature review yields a similar observation that most existing models focus on assessment and comparison of *apriori* defined strategies, and virtually none of the models are capable of *"learning"*, i.e., adapting to changes in the pandemic progress, or even predicting them, to generate *dynamic* strategies. Such a strategy has the advantage of being developed as the pandemic spreads, by generating mitigation decisions at each decision epoch, based on both the present state of the pandemic and its expected evolution.

In an attempt to address the IOM recommendations, we present a simulation optimization model for generating dynamic resource distributions over a network of regional outbreaks. The simulation model mimics the disease and population dynamics of the affected regions (§ 3.1, 3.2). As the pandemic spreads from region to region, the optimization model distributes mitigation resources, such as stockpiles of vaccines and antiviral, and administration capacities (§ 3.3). The model seeks to minimize the impact of ongoing outbreaks and the expected impact of *potential* outbreaks, using measures of morbidity, mortality, and social distancing, translated into the cost of lost productivity and medical services.

The model has the ability to *redistribute* the resources remaining from previous allocations based on the current pandemic status and its expected evolution. This allows a more efficient utilization of resources compared to irrevocable distributions in which allocated resources remain in the regions regardless the posterior course of the pandemic. Our methodology is implemented on a simulated H5N1 outbreak covering four counties in Florida, U.S., with over four million inhabitants (§ 4). The performance of the strategy is compared to that of a reactive myopic distribution policy, which allocates resources from one *actual* outbreak region to the next, each time trying to cover the *entire* regional population at risk, regardless of both resource availability and projected pandemic evolution.

Compared to our earlier work [35], this paper presents the following advances: (i) the original single-region simulation has been expanded to serve as the basis for the cross-regional simulation model, and (ii) the paper presents a dynamic optimization model to generate resource (re)distribution strategies. As such, the decision support power of our model has substantially increased.

3. Methodology

Our methodology generates dynamic progressive strategies for distribution of limited mitigation resources over a network of regional outbreaks. It incorporates: (i) a cross-regional simulation model, (ii) a set of single-region simulation models, and (iii) an optimization model.

We consider a network of regions each of which classified as either unaffected, ongoing, or contained outbreak (Fig. 1). The cross-regional simulation model connects the regions by air and land travel. The single-region simulation models mimic the population and disease dynamics of each ongoing region, impacted by intervention measures. A pandemic can spread from ongoing to unaffected regions by infectious travelers who pass through the regional border control. As a new regional outbreak occurs, the optimization model allocates available resources to the new outbreak region (*actual distribution*) and unaffected regions (*virtual distribution*). Detailed daily statistics are collected for each ongoing

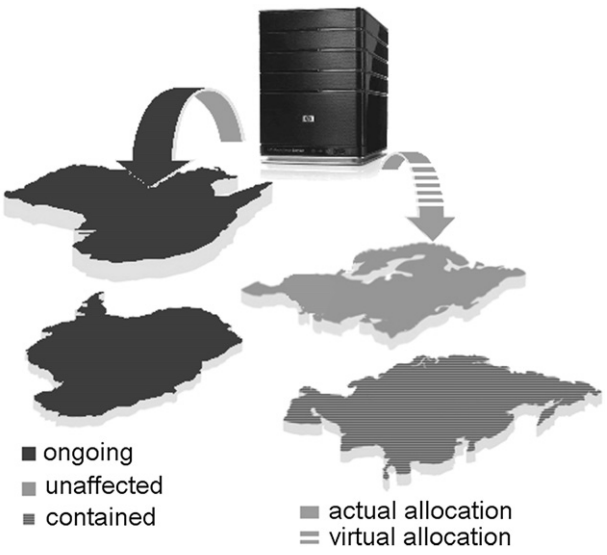

Fig. 1. A schematic of cross-regional pandemic spread and resource distribution.

region. When a regional outbreak is contained, its societal and economic costs are calculated.

3.1. Cross-regional simulation model

A schematic of the cross-regional simulation model is shown in Fig. 2. The model is initialized by creating population entities and mixing groups for each network region. A pandemic is triggered by an infectious case injected into a randomly selected region. This case starts circulating through the mixing groups coming into contacts with susceptible inhabitants. The details of the resulting contact dynamics and infection transmission are given in Section 3.2. As the infected cases start seeking medical help, a new regional outbreak is detected. A resource distribution is then determined and resources, if any, are provided to the region. The outbreak can spread to unaffected regions as some infectious travelers pass through the regional border control. By tracing these travelers, the model determines which of the unaffected regions, if any, become new regional outbreaks. The model also determines if any regional outbreaks have been contained. The simulation stops when all regional outbreaks are contained.

3.2. Single-region simulation model

The single-region model includes the following components (see Fig. 3): (i) mixing groups and schedules, (ii) contact and infection process, (iii) disease natural history, and (iv) mitigation strategies, which include pharmaceutical and non-pharmaceutical interventions. The model collects detailed daily statistics, including number of infected, recovered, deceased, and quarantined cases, for different age groups. The model also calculates the societal and economic costs for each contained regional outbreak. The societal cost includes the cost of lost lifetime productivity of the deceased; the economic cost includes the cost of medical expenses of the recovered and deceased and the cost of lost productivity of the quarantined [68].

3.2.1. Mixing groups and schedules

Each region is modeled as a set of community centers formed by *mixing groups* or places where individuals come into contact with each other during the course of their social interactions. Examples of mixing groups include households, offices, schools, universities, shopping centers, entertainment centers, etc. [35]. Each individual is assigned a set of attributes such as age, gender, parenthood, workplace, infection susceptibility, and probability of travel, among others. Each person is also assigned Δt-time discrete weekday and weekend schedules ($\Delta t = 1$ h, for example), which depend on: (i) age, parenthood, and employment status, (ii) disease status, (iii) travel status, and (iv) compliance to social distancing decrees. Examples of schedules can be found in Ref. [69]. Based on their schedules, the individuals circulate in the mixing groups and come into contact with others (see § 3.2.2 for details).

It is assumed that at any point of time, an individual belongs to one of the following compartments (Fig. 4): susceptible, contacted (by an infectious individual), infected (asymptomatic or symptomatic), and recovered/deceased. In what follows, we present the infection transmission and disease natural history models, which describe the transitions between the above compartments.

3.2.2. Contact and infection transmission

Infection transmission occurs during contact events in the mixing groups between susceptible and infectious cases. At the

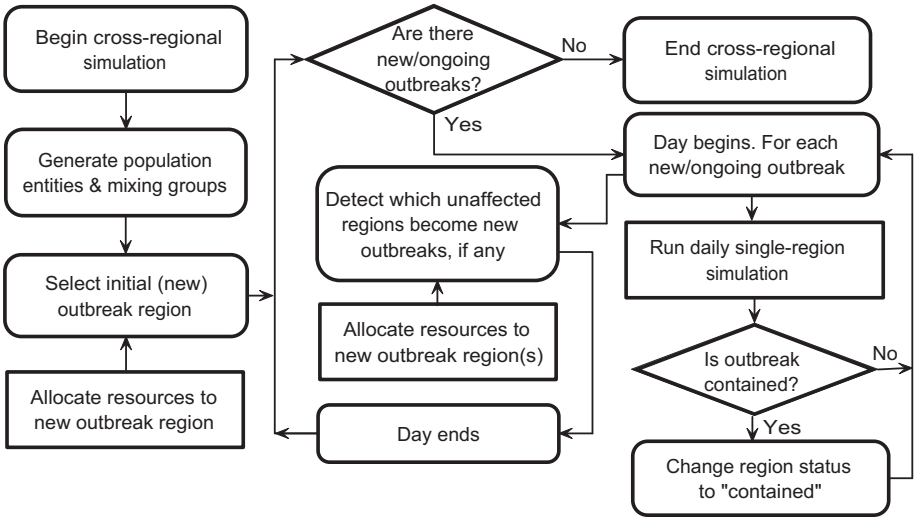

Fig. 2. Schematic of the cross-regional simulation model.

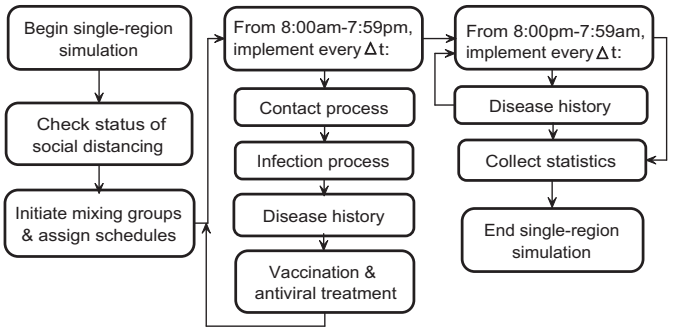

Fig. 3. Schematic of the single-region simulation model.

beginning of each period Δt (e.g., 1 h), for each mixing group g, the simulation tracks the total number of infectious cases present in the group. It is assumed that each infectious case generates r_g new contacts per Δt unit of time [37]. The contacts are chosen randomly (uniformly) from the pool of susceptible present in the group. We also assume the following: (i) during Δt period, a susceptible may come into contact with at most one infectious case and (ii) each such contact exposure lasts Δt units of time. Once a susceptible has started her contact exposure at time t, she will develop infection at time $t+\Delta t$ with a certain probability that is calculated as shown below.

Let $L_i(t)$ be a nonnegative continuous random variable that represents the duration of contact exposure, starting at time t, required for susceptible i to become infected. We assume that $L_i(t)$ is distributed exponentially with mean $1/\lambda_i(t)$, where $\lambda_i(t)$ represents the instantaneous force of infection applied to susceptible i at time t [70,71]. The probability that susceptible i, whose contact exposure has started at time t, will develop infection at time $t+\Delta t$ is then given as

$$P\{L_i(t) \le \Delta t\} = 1 - e^{-\lambda_i(t)\Delta t}. \quad (1)$$

3.2.3. Disease natural history

Once infected, an individual simultaneously enters the periods of latency and incubation (Fig. 5). At the end of the latency phase, the individual enters the infectious phase [37,64]. The infected becomes symptomatic at the end of the incubation period. Following the infectious phase, the individual enters the period leading to a health outcome, which culminates in a recovery or death.

Mortality for influenza diseases is a complex process affected by many factors and variables, most of which have limited accurate data support available from past pandemics. Furthermore, the time of death can sometimes be weeks following the disease episode (which is often attributable to pneumonia related complications [72]). Because of the uncertainty underlying the mortality process,

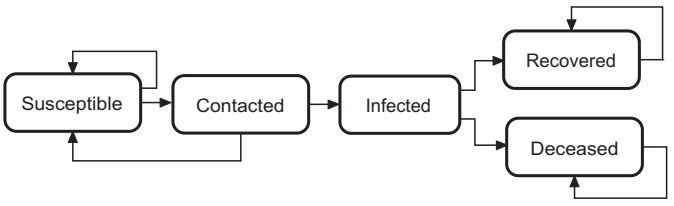

Fig. 4. Schematic of disease natural history model.

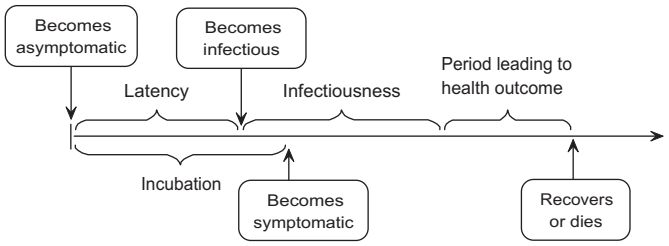

Fig. 5. Schematic of disease natural history model.

we adopted an age-based form of the mortality probability of infected i, as follows

$$m_i = \mu_i(1 - \tau\rho_i), \quad (2)$$

where μ_i is the age-dependent *base* mortality probability of infected i, ρ_i is the status of antiviral treatment (0 or 1), and τ denotes the antiviral efficacy measured through the relative decrease in the base mortality probability [62]. It is assume that a recovered case develops full immunity to the virus strain and continues circulating in the mixing groups based on her regular daily schedule.

3.2.4. Mitigation strategies

Mitigation options include pharmaceutical and non-pharmaceutical interventions. Mitigation is initiated upon detection of a threshold number of confirmed infected cases [73], which triggers resource distribution and deployment. Our model incorporates a certain delay for field deployment.

Pharmaceutical interventions include vaccination and antiviral application. Vaccination is targeted at individuals at risk [74] to reduce their susceptibility. It takes a certain amount of time for the vaccine to become effective [75]. Vaccination is constrained by the allocated stockpile and administration capacity, measured in terms of the immunizer-hours. We assume that as some infected cases seek medical help [76,77], those at risk will receive the antiviral. Antiviral application is constrained by the allocated stockpile and administration capacity, measured in terms of the number of certified providers.

Both vaccination and antiviral application are affected by a number of socio-behavioral factors, including conformance of the target population, degree of risk perception, and compliance of healthcare personnel [78–80]. The conformance level of the population at risk can be affected, among other factors, by the demographics and income level [81–85] as well as by the quality of public information available [86]. The degree of risk perception can be influenced by the negative experiences developed during previous pharmaceutical campaigns [87,88] as well as by public fear and rumors [89,90].

Non-pharmaceutical interventions include social distancing and travel restrictions. We adopted a CDC guidance [67], which establishes five categories of pandemic severity and recommends quarantine and closure options for each category. The categories are defined by the value of the case fatality ratio (CFR), which is the proportion of fatalities in the total infected population. For CFR values lower than 0.1% (category 1), voluntary at-home isolation of infected cases is implemented. For CFR values between 0.1% and 1.0% (categories 2 and 3), in addition to at-home isolation, the following measures are *recommended*: (i) voluntary quarantine of household members of infected cases and (ii) child and adult social distancing. For CFR values exceeding 1.0% (categories 4 and 5), all the above measures are *implemented*. As the effectiveness of social distancing is affected by some of the socio-behavioral factors listed above [86], we assume a certain social distancing conformance

level. Travel restrictions considered in our model include regional air and land border control for infected travelers.

3.3. Optimization model

Optimization model is invoked at the beginning of every regional outbreak epoch (episode) $n = 1, 2, \ldots$, starting with the initial outbreak ($n = 1$). The objective of the model is to allocate some of the available mitigation resources to the new outbreak region (called actual distribution) while reserving the rest for potential outbreak regions (called virtual distribution). By doing so, the model seeks to progressively minimize the impact of ongoing outbreaks and the expected impact of potential outbreaks. The model is able to *redistribute* the resources remaining from previous allocations in response to changes in the current pandemic status and its expected evolution. Mitigation resources can include stockpiles of vaccines and antivirals, administration capacity, hospital beds, and personal protective equipment, among others. In what follows, we present the construction of the optimization model followed by the dynamic predictive algorithm for the cross-regional simulation optimization methodology.

We introduce the following *general notation*.

S = set of all network regions,

A^n = set of regions in which pandemic is contained by the n^{th} outbreak epoch,

B^n = set of ongoing outbreak regions at the n^{th} outbreak epoch,

C^n = set of unaffected regions at the n^{th} outbreak epoch,

R = set of available types of mitigation resources ($R = \{1, 2, \ldots, r\}$),

q^n_{ik} = amount of resource i allocated to region k at the n^{th} outbreak epoch,

$Q_i{}^n$ = total availability of resource i at the n^{th} outbreak epoch (including quantities from previous allocations which have not been used up),

H = set of age groups.

The objective function of the optimization model will incorporate measures of expected societal and economic costs of the pandemic. The societal cost includes the cost of lost lifetime productivity of the deceased. The economic cost includes the cost of medical services provided to the recovered and deceased and the cost of lost productivity of the quarantined. To estimate these costs, the following *impact measures* of morbidity, mortality, and quarantine are calculated for each region k:

X_{hk} = total number of infected cases in age group h who seek medical assistance,

Y_{hk} = total number of infected cases in age group h who do not seek medical assistance,

D_{hk} = total number of deceased cases in age group h,

V_{hk} = total number of person-days of cases in age group h who comply with quarantine.

We estimate the above impact measures as a function of amounts of resources using the following nonlinear regression models obtained from single-region simulation of each region k:

$$X_{hk} = \delta^0_{hk} + \sum_{i \in R} \delta^i_{hk} \cdot q_{ik} + \sum_{i,m \in R,\ i \neq m} \delta^{im}_{hk} \cdot q_{ik} \cdot q_{mk}, \tag{3}$$

where $\delta^0_{\cdot\cdot}$ represents the intercept, $\delta^i_{\cdot\cdot}$ denotes the regression coefficient associated with resource i, and $\delta^{im}_{\cdot\cdot}$ is the regression coefficient for the interaction between resources i and m. In the above model, the product terms account for the correlated contribution of the resources to the impact measures. Statistical significance of such correlated contributions was obtained in preliminary numerical experiments. Similar regression models are used for Y_{hk}, D_{hk}, and V_{hk}.

The regression equations are developed using single-region simulation models, assuming region k is the initial outbreak region. However, since the disease infectivity subsides as the pandemic evolves, the regression coefficients need to be re-estimated at every new outbreak epoch, for each region $k \in B^n \cup C^n$, using single-region simulation models. These simulations ought to be initialized to the current outbreak status in region k per the cross-regional simulation.

We use a regression model to estimate the probability p_{lk} of pandemic spread from affected region l to unaffected region k. The probability is expressed as a function of resources allocated to region l, which influences the number of outgoing infectious travelers from region l to k, and is given as

$$p_{lk} = \gamma^0_{lk} + \sum_{i \in R} \gamma^i_{lk} \cdot q_{il} + \sum_{i,m \in Ri \neq m} \gamma^{im}_{lk} \cdot q_{il} \cdot q_{ml}, \tag{4}$$

where $\gamma_{\cdot\cdot}{}^0$ represents the intercept, $\gamma_{\cdot\cdot}{}^i$ denotes the regression coefficient associated with resource i, and $\gamma_{\cdot\cdot}{}^{im}$ is the regression coefficient associated with interaction between resources i and m. The regression equation considers region k as the initial outbreak region. To estimate the probability $p_{lk}{}^n$ of pandemic spread from affected region l to unaffected region k at the n^{th} outbreak epoch, the regression coefficients in 4 need to be re-estimated as in the case of the impact measures. The total outbreak probability for unaffected region k at the n^{th} outbreak epoch is calculated as $p^n_k = \sum_{l \in B^n} p^n_{lk}$.

Finally, we calculate the total cost of an outbreak in region k at the n^{th} outbreak epoch as follows

$$TC^n_k = \sum_{h \in H} (m_h + \overline{w}_h) X^n_{hk} + \sum_{h \in H} \overline{w}_h \cdot Y^n_{hk} + \sum_{h \in H} \widehat{w}_h \cdot D^n_{hk} + \sum_{h \in H} w_h \cdot V^n_{hk}, \tag{5}$$

where

m_h = total medical cost of an infected case in age group h over his/her disease period,

$\overline{w}_h$ = total cost of lost wages of an infected case in age group h over his/her disease period,

$\widehat{w}_h$ = cost of lost lifetime wages of a deceased case in age group h,

w_h = daily cost of lost wages of a non-infected case in age group h who complies with quarantine.

3.3.1. The model

The optimization model invoked at the n^{th} outbreak epoch ($n = 1, 2, \ldots$) has the following form.

$$\text{Minimize } TC^n_j\left(q^n_{1j}, q^n_{2j}, \ldots, q^n_{rj}\right) + \sum_{l \in B^n \setminus \{j\}} TC^n_l\left(q^n_{1l}, q^n_{2l}, \ldots, q^n_{rl}\right) + \sum_{s \in C^n} TC^n_s\left(q^n_{1s}, q^n_{2s}, \ldots, q^n_{rs}\right) \cdot p^n_s$$

$$\text{subject to} \quad q^n_{ij} + \sum_{l \in B^n \setminus \{j\}} q^n_{il} + \sum_{s \in C^n} q^n_{is} \cdot p^n_s \leq Q^n_i \quad \forall i \in R,$$

$$q^n_{ij}, q^n_{il}, q^n_{is} \geq 0 \quad \forall i \in R.$$

The first term of the objective function represents the total cost of the new outbreak j, estimated at the n^{th} outbreak epoch, based on an actual resource distribution $\{q^n_{1j}, q^n_{2j}, \ldots, q^n_{rj}\}$ (see Eq. (5). The second term represents the total cost of ongoing outbreaks (excluding region j), re-estimated at the n^{th} outbreak epoch, to capture any changes in the status of ongoing regions. The third term

represents the total expected cost of outbreaks in currently unaffected regions, based on a virtual distribution $\{q^n_{1s}, q^n_{2s}, \ldots, q^n_{rs}\}$ and the regional outbreak probabilities $p_s{}^n$. The set of constraints assures that for each resource i, the total (nonnegative) quantity allocated does not exceed the total resource availability.

3.4. Dynamic predictive simulation optimization (DPO) algorithm

1. Estimate regression equations for each region using the single-region simulation model (Eq. (3) and (4)).
2. Begin the cross-regional simulation model.
3. Initialize the sets of regions: $A^n = \emptyset$, $B^n = \emptyset$, $C^n = S$.
4. Select randomly the initial outbreak region j. Set $n = 1$.
5. Update sets $B^n \leftarrow B^n \cup \{j\}$ and $C^n \leftarrow C^n \setminus \{j\}$.
6. Solve the optimization model at the n^{th} outbreak epoch. Update resource availabilities.
7. If $B^n \neq \emptyset$, go to step 8. Else, go to step 11.
8.
   (a) For each ongoing region, implement a next day run of its single-region simulation.
   (b) Check the containment status of each ongoing region. Update sets A^n and B^n, if needed.
   (c) For each unaffected region, calculate its outbreak probability.*
   (d) Determine if there is a new outbreak region(s) j. If there is no new outbreak(s), go to step 7. Otherwise, go to step 9.
9. For each new outbreak region j:
   (a) Increment $n \leftarrow n + 1$.
   (b) Update sets $B^n \leftarrow B^n \cup \{j\}$ and $C^n \leftarrow C^n \setminus \{j\}$
   (c) Re-estimate regression equations for each region $k \in B^n \cup C^n$, where each single-region simulation is initialized to the current outbreak status in the region.
   (d) Solve the optimization model at the n^{th} outbreak epoch. Update resource availabilities.
10. Go to step 7.
11. Calculate the total cost for each contained region and update the overall pandemic cost.

* The probability is determined based on the number of infectious travelers present in the region. Travelers are considered to act independently. Each infectious traveler is assumed to trigger an outbreak with an equal and time-homogeneous probability for the entirety of his/her infectious period. The total outbreak probability is then determined using the binomial probability model. A uniformly (0,1) distributed random variable is then generated to determine whether an outbreak occurs or not.

4. Testbed illustration

To illustrate the use of our DPO methodology, we implemented a sample H5N1 outbreak scenario including four counties in Florida: Miami Dade, Hillsborough, Duval, and Leon. The counties contain four major and densely populated metropolitan areas and transportation hubs of the state: Miami, Tampa, Jacksonville, and Tallahassee, respectively (see Fig. 6). The respective populations of these counties are 2.2, 1.0, 0.8, and 0.25 million people. A basic unit of time for population and disease dynamics models was taken to be $\Delta t = 1$ h. Regional simulations were run for a period (up to 180 days) until the daily infection rate approached near zero (see Section 4.3). Below we present the details on selecting model parameter values. Most of the testbed data can be found in the supplement [69].

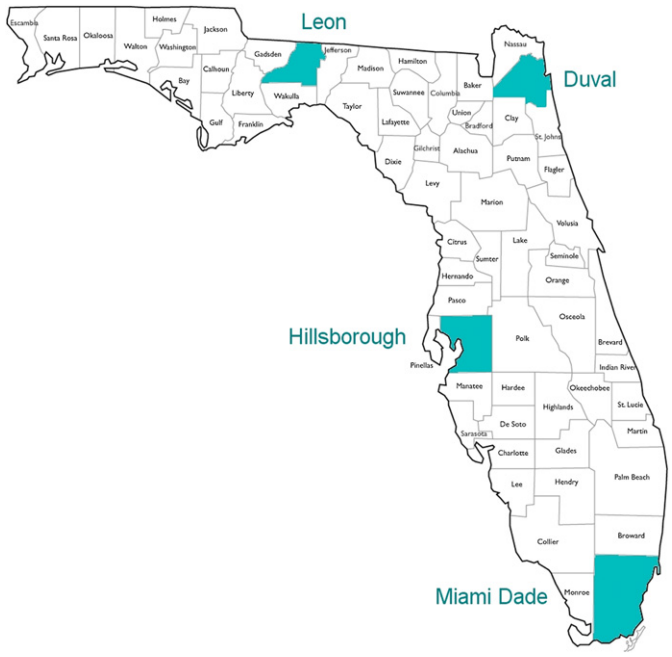

Fig. 6. Testbed counties in FL.

4.1. Parameter values for population and disease dynamics models

Demographic and social dynamics data for each region (see Ref. [69]) were taken from the U.S. Census [91] and the National Household Travel Survey [92]. Hourly schedules (see Ref. [69]) were adopted from [35].

Each infected person was assigned a daily travel probability 0.0024 [92], of which 7% by air and 93% by land. The probabilities of travel destinations among the four regions (see Table 1) were calculated using traffic volume data [93–96]. We assumed that symptomatic travelers were detected at the border check points with probabilities 0.95 and 0.90, for air and land travel, respectively [97].

We modeled the instantaneous force of infection applied to contact i at time t (see Eq. (1) as follows (see also Fig. 7):

$$\lambda_i(t) = -\ln(1 - p_i(t)), \tag{6}$$

where $p_i(t) = \alpha_i - \delta\theta_i(t)$ is the effective probability of contact i getting infected during a contact exposure of unit length ($\Delta t = 1$) that began at time t during the pandemic evolution. The elements α_i denote the age-dependent base infection probability of contact i, $\theta_i(t)$ is the status of vaccination at time t (0 or 1), and δ is the vaccine efficacy, measured as the reduction in the base infection probability (achieved in 10 days following vaccination [75]).

The values of age-dependent base infection probabilities were adopted from (37) (see Table 2). We considered disease natural history with a latent period of 29 h (1.21 days), an incubation period

Table 1
Inter-regional travel probabilities.

Origin\Destination	Inter-regional travel probability			
	Hillsborough	Miami D.	Duval	Leon
Hillsborough	0.00	0.60	0.27	0.13
Miami D.	0.74	0.00	0.16	0.10
Duval	0.61	0.29	0.00	0.10
Leon	0.52	0.31	0.17	0.00

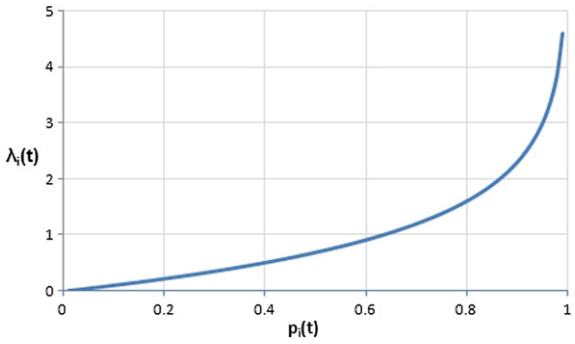

Fig. 7. Instantaneous force of infection.

of 46 h (1.92 days), an infectiousness period from 29 to 127 h (1.21–5.29 days), and a period leading to health outcome from 127 to 240 h (5.29–10 days) [98].

Base mortality probabilities (μ_i in Eq. (2) were found using the statistics recommended by the Working Group on Pandemic Preparedness and Influenza Response [68]. The statistics shows the percentage of mortality for age-based high-risk cases (HRC) (Table 3, columns 1–3). Mortality probabilities (column 4) were estimated under the assumption that fatalities from the high-risk cases account for 85% of the total number of fatalities for each age group [68].

4.2. Calibration of the single-region models

Single-region simulation models were calibrated using two common measures of pandemic severity [33,34,37]: the basic reproduction number (R_0) and the infection attack rate (*IAR*). R_0 is defined as the average number of secondary infections produced by a typical infected case in a totally susceptible population. *IAR* is defined as the ratio of the total number of infections over the pandemic period to the size of the initial susceptible population. To determine R_0, all infected cases inside the simulation were classified by generation of infection, as in [36,41]. The value of R_0 was calculated as the average reproduction number of a typical generation in the early stage of the pandemic, with no interventions implemented (*the baseline* scenario) [41]. Historically, R_0 values for PI ranged between 1.4 and 3.9 [36,57]. To attain similar values, we calibrated the hourly contact rates of mixing groups [69] (original rates were adopted from [37]). For the four regions, the average baseline value of R_0 was 2.54, which represented high transmissibility scenarios. The values of regional baseline *IAR* averaged 0.538.

4.3. Parameters of mitigation

Mitigation resources included stockpiles of vaccines and antiviral and administration capacities. A 24-h delay was assumed for deployment of resources and field responders [73].

Pharmaceutical interventions. The vaccination risk group included healthcare providers [80] and individuals younger than 5 years (excluding younger than 12 months old) and older than 65 years [74]. The risk group for antiviral included symptomatic individuals below 15 years and above 55 years [74,99]. The efficacy levels for the vaccine (δ in Eq. (6) and antiviral (τ in Eq. 2) were assumed to be 40% and 70%, respectively [62,100]. We did not consider the use of antiviral for a mass prophylaxis because of the limited antiviral availability [15] and the risk of emergence of antiviral resistant transmissible virus strains [54]. We assumed a 90% target population conformance for both vaccination and antiviral treatment [78]. The immunity development period for the vaccine was taken as 10 days [75].

Non-pharmaceutical interventions. A version of the CDC guidance on non-pharmaceutical interventions [67] for Category 5 was implemented (§ 3.2.4). Once the reported (observed) CFR value had reached 1.0%, the following policy remained in effect for 14 days as in [67]: (i) individuals below a certain age (22 years) stayed at home during the entire policy duration, (ii) of the remaining population, a certain proportion ϕ [101] stayed at home and was allowed a one-hour leave, every three days, to buy essential supplies, and (iii) the remaining $(1-\phi)$ non-compliant proportion followed their regular schedule. All testbed scenarios considered the quarantine conformance level ϕ equal to 80% [86]. The initiation threshold for social distancing was taken as 1000 confirmed infected cases [64].

An outbreak was considered contained if the daily infection rate did not exceed five cases for seven consecutive days. Once contained, a region was simulated for an additional 10 days to allow the remaining infected cases complete their disease natural history. A 2^5 statistical design of experiment [102] was used to develop the regression equations discussed in § 3.3 (the values of adjusted R^2 ranged from 96.36% to 99.97%). The simulation code was developed using C++. The running time for a cross-regional simulation replicate involving over four million inhabitants ranged between 17 and 26 min on a Pentium 3.40 GHz with 4.0 GB of RAM. A total of 150 replicates were run for each scenario.

For the testbed discussed in the paper, nonlinear regression models were used to capture the correlated contribution of different types of mitigation resources to the impact measures. Statistical significance of such correlated contributions was established during preliminary numerical experiments. As such, the resulting optimization model was nonlinear as the objective function and constraints contained second order product terms. However, the model itself was small since the number of decision variables and constraints was determined by the number of resource types (e.g., antivirals, vaccines, etc.) and the cardinality of the sets of ongoing and unaffected regions. To solve the optimization model, we used Lingo 12.0 professional version and

Table 2
Base infection probabilities [37].

Age group	0–5	6–19	20–29	31–65	66–99
α_i	0.156	0.106	0.205	0.195	0.344

Table 3
Base mortality probabilities.

Age group	% HRC	% Mortality in HRC	μ_i
0–19	6.4	9.0	0.007
20–64	14.4	40.9	0.069
65+	40.0	34.4	0.162

Table 4
Total and regional resource requirements.

Region (population)	Resource requirements by region				
	Hillsb. (1,007,916)	Miami D. (2,209,702)	Duval (852,168)	Leon (248,761)	Total (4,318,547)
Resource					
Vaccine stockpile	305,036	679,181	241,522	76,007	1,301,745
Antiviral stockpile	415,294	749,058	460,393	105,307	1,730,052
No. antiv. nurses	650	1104	786	166	2706
No. vacc. nurses	1059	2358	839	264	4520

Table 5
Values of pandemic impact measures (societal and economic costs).

Pandemic impact measure (age group, years)	Value US$
Average cost of lost lifetime productivity of a deceased case (0–19)	$1,336,347.86
Average cost of lost lifetime productivity of a deceased case (20–64)	$1,370,987.28
Average cost of lost lifetime productivity of a deceased case (65–99)	$98,959.24
Average cost of lost productivity and medical expenses of a recovered/deceased case (0–19)	$5,078.48
Average cost of lost productivity and medical expenses of a recovered/deceased case (20–64)	$10,466.68
Average cost of lost productivity and medical expenses of a recovered/deceased case (65–99)	$11,566.09
Average daily cost of lost productivity of a non-infected quarantined case (20–99)	$432.54

benchmarked the results against pro-rata resource distributions which allocated resources to the regions in proportion of their population. In the next section, we compare the performance of DPO strategy to that of a reactive myopic policy.

4.4. Comparison of DPO and myopic strategies

The myopic policy allocates resources to each *actual* outbreak region in the amount of *total* regional resource requirements (see table below) subject to total resource availability. Such reactive resource distribution is similar to the "first some, first served" principle whereby early outbreak regions will always have priority over later regions regardless of projected pandemic evolution. The performance of the DPO and myopic policies is compared at different levels of the total resource availability.

Table 4 summarizes the total vaccine and antiviral requirements for each region, based on the composition of the regional risk groups (see § 4.3). Table 5 shows the per capita costs of lost productivity and medical expenses, which were adopted from [68] and adjusted for inflation for the year of 2010 [103].

Comparison of the two strategies is done at the levels of 20%, 50%, and 80% of the total resource requirement shown in Table 4. Figs. 8(a) and (b) show the policy comparison in the form of the 95% confidence intervals (CI) for the average number of infected and deceased, respectively.

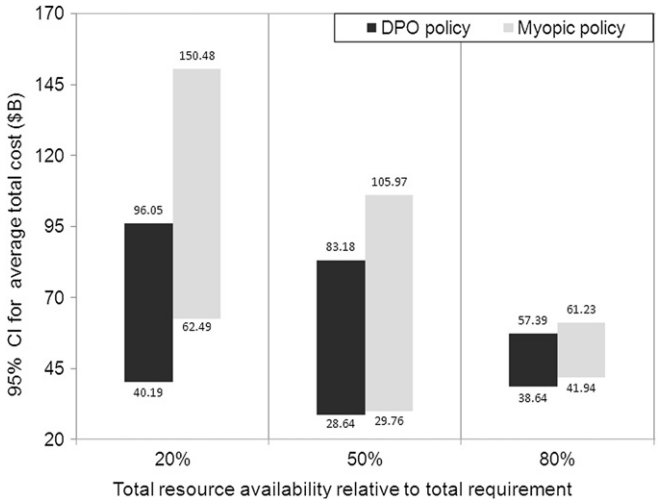

Fig. 9. DPO vs. myopic (total cost).

Fig. 9 also shows the policy comparison using the 95% CI for the average total pandemic cost, calculated using the pandemic statistics and the per capita costs from Table 5. For illustrative purposes, we also show the average number of regional outbreaks, for each policy, at different levels of resource availability, in the testbed scenario involving four regions, with the Hillsborough as the initial outbreak region (Table 6).

It can be observed that the values of all impact measures exhibit a downward trend, for both DPO and myopic policies, as the total resource availability increases from 20% to 80%.

An increased total resource availability not only helps alleviating the pandemic impact inside the ongoing regions but also reduces the probability of spread to the unaffected regions. For both policies, as the total resource availability approaches the total resource requirement (starting from approximately 60%), the impact numbers show a converging behavior, whereby the marginal utility of additional resource availability diminishes. This behavior can be explained by noting that the total resource requirements were determined assuming the worst case scenario when *all* (four) regions would be affected and ought to be provided with enough resources to cover their respective regional populations at risk.

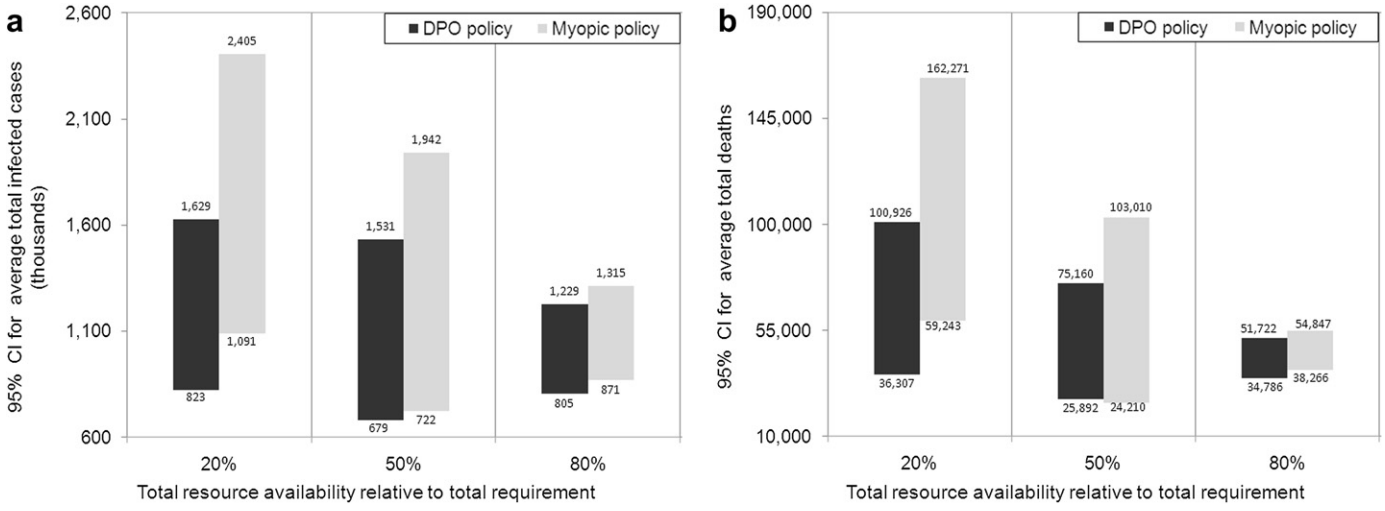

Fig. 8. Comparison of DPO and myopic policies (average number infected 8(a) and deaths 8(b)).

Table 6
Average number of regional outbreaks for DPO and myopic policies.

	Total resource availability		
Policy	20%	50%	80%
DPO	1.75	1.66	1.44
Myopic	2.40	1.77	1.50

It can also be seen that on average, the DPO policy outperforms the myopic approach at all levels, which can attest to a more efficient resource utilization achieved by the DPO policy (see also Table 6). The difference in the policy performance is particularly noticeable at the lower levels of resource availability and it gradually diminishes, as the resource availability increases and becomes closer to be sufficient to cover the entire populations at risk in all regions. It can also be noted that the variability in the performance of the DPO strategy is generally smaller than that of the myopic policy. In general, for both strategies, the performance variability decreases with higher availability of resources.

4.5. Sensitivity analysis

In this section, we assess the marginal impact of variability of some of the critical factors. The impact was measured separately by the change in the total pandemic cost and the number of deaths (averaged over multiple replicates), resulting from a unit change in a decision factor value, one factor at a time. Factors under consideration included: (i) antiviral efficacy, (ii) social distancing conformance, and (iii) CDC response delay. We have used all four regions, separately, as initial outbreak regions for each type of sensitivity analysis. The results (patterns) were rather similar. Due to limited space, we have opted to show the results for only one initial region, chosen arbitrarily, for each of the three types of sensitivity studies. While Duval County was selected as the initial outbreak region to show the sensitivity results on antiviral efficacy, Hillsborough and Miami Dade were used as the initial regions to show the results on respectively social distancing conformance and CDC response delay.

4.5.1. Antiviral efficacy

Fig. 10 depicts the sensitivity of the average total cost and average total deaths to antiviral efficacy values between 0% and 80%. As expected, for both policies, the curves for the average number of deaths exhibit a decreasing trend which is almost linear for the values of τ between 0% and 40%. As the value of τ approaches 70%, the curves start exhibit a converging behavior. The curves for the average total pandemic cost exhibit a similar pattern for both policies.

It can be noted that the performance of both policies is somewhat identical for low antiviral efficacy (between 0% and 30%). However, the performance of the DPO policy improves consistently as τ increases which can be attributed to a more discretionary allocation of the antiviral stockpile.

4.5.2. Social distancing conformance

Reduction of the contact intensity through quarantine and social distancing has proven to be one of the most effective containment measures, especially in the early stages of the pandemic (29, 30, 32, 60). Fig. 11 shows the sensitivity of the average total cost and average total deaths to the social distancing conformance ranging between 60% and 80%.

We observed that for both impact measures, the DPO policy demonstrated a significantly better performance than the myopic policy with the difference ranging from \$3B to \$26B in the total cost and from 1400 to 20,000 in the number of fatalities. The biggest difference in performance was achieved at the lower-to-medium levels of conformance (65–72%). As the conformance level approached 80%, the dominating effect of social distancing masked the effect of a better utilization of vaccines and antiviral agents achieved by the DPO strategy.

4.5.3. CDC response delay

The CDC response delay corresponds to the interval of time from the moment an outbreak is detected to a complete deployment of mitigation resources. Depending on the disease infectivity, CDC response delay may represent one of the most critical factors in the mitigation process.

Fig. 12 shows how the performance of both policies was significantly impacted by this factor. The DPO policy showed a uniformly better performance with the difference ranging between \$3B to \$4B in the average total cost, and between 800 and 1800 in the average number of mortalities, over the range (24–72 h) of the response delay that we examined. For both policies, there was no significant difference when the delay was between 24 and 48 h. However, for the delay values exceeding 48 h, the average number of deaths and total cost increased at a high rate.

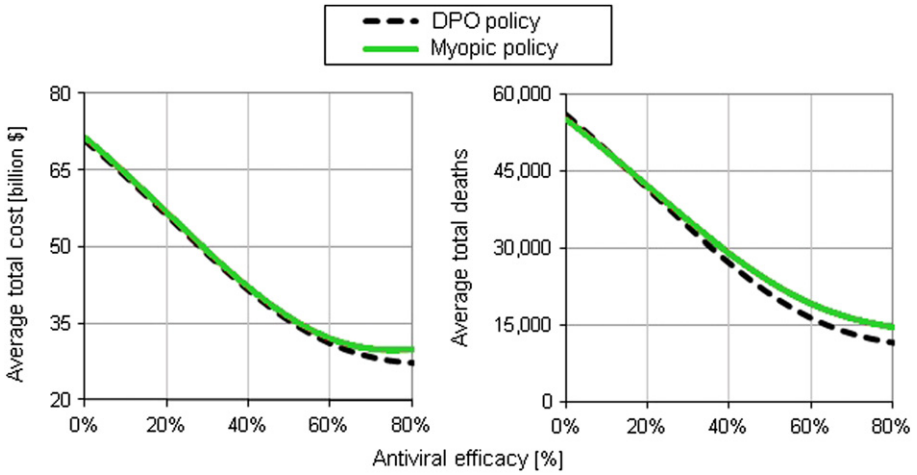

Fig. 10. Sensitivity analysis for antiviral efficacy.

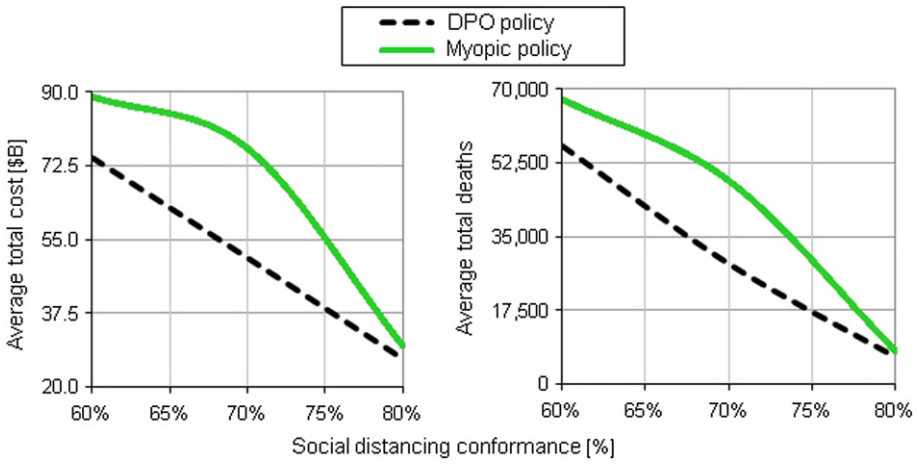

Fig. 11. Sensitivity analysis for quarantine conformance.

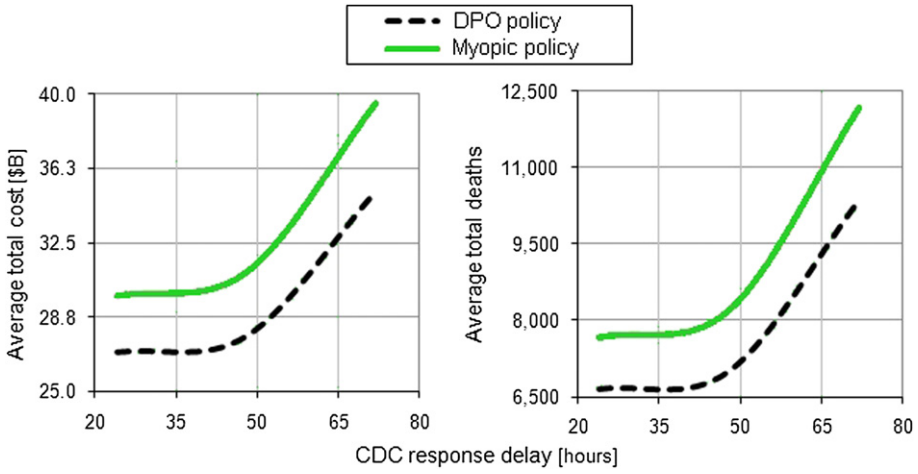

Fig. 12. Sensitivity analysis for CDC response delay.

5. Conclusions

A recent report by the Institute of Medicine points out that the existing models for PI mitigation fall short of providing *dynamic* decision support. The report recommends "that policymakers consider a broader set of models to inform strategies and policies regarding pandemic influenza" [66]. In this paper, we present a large-scale simulation optimization model which attempts to fill this gap.

The model supports dynamic predictive resource distribution over a network of regions exposed to the pandemic. The model aims to balance both the ongoing and potential outbreak impact, which is measured in terms of morbidity, mortality, and social distancing, translated into the cost of lost productivity and medical expenses. The model was calibrated using historic pandemic data and compared to the myopic strategy, using a sample outbreak in FL, U.S., with over 4 million inhabitants.

Summary of the main results. For both strategies, the marginal utility of additional resource availability was found to be diminishing, as the total resource availability approached the total requirement.

In the testbed scenario, the DPO strategy on average outperformed the myopic policy. As opposed to the DPO strategy, the myopic policy is reactive, rather than predictive, as it allocates resources regardless of the remaining availability and the overall cross-regional pandemic status. Hence is the name myopic. In contrast, the DPO model distributes resources trying to balance the impact of actual outbreaks and the expected impact of potential outbreaks. It does so by exploiting region-specific effectiveness of mitigation resources and dynamic reassessment of pandemic spread probabilities, using a set of regression submodels. Hence, we believe that in scenarios involving regions with a more heterogeneous demographics, the DPO policy will likely perform even better and with less variability than the myopic strategy. We also note that the difference in the model performance was particularly noticeable at lower levels of resource availability, which is in accordance with a higher marginal utility of additional availability at that levels. We thus believe that the DPO model can be particularly useful in scenarios with very limited resources.

Contributions of the paper. The methodology presented in this paper is one of the first attempts to offer *dynamic predictive* decision support for pandemic mitigation, which incorporates measures of societal and economic costs. Our comparison study of the DPO vs. myopic cross-regional resource distribution is also novel. Additionally, our simulation model represents one of the first of its kind in considering a broader range of social-behavioral aspects, including vaccination and antiviral treatment conformance. The simulation features a flexible design which can be

particularized to a broader range of pharmaceutical and non-pharmaceutical interventions and even more granular mixing groups.

We also developed a decision-aid simulator which is made available to the general public through our web site at http://imse.eng.usf.edu/pandemics.aspx. The tool is intended to assist public health decision makers in implementing what-if analysis for assessment of mitigation options and development of policy guidelines. Examples of such guidelines include vaccine and antiviral risk groups, social distancing policies (e.g., thresholds for declaration/lifting and closure options), and travel restrictions.

Limitations of the model. Lack of reliable data prevented us from considering geo-spatial aspects of mixing group formation. We also did not consider the impact of public education and the use of personal protective measures (e.g., face masks) on transmission, again due to a lack of effectiveness data [104]. We did not study the marginal effectiveness of individual resources due to a considerable uncertainty about the transmissibility of an emerging pandemic virus and efficacy of vaccine and antiviral. For the same reason, the vaccine and antiviral risk groups considered in the testbed can be adjusted, as different prioritization schemes have been suggested. The form of social distancing implemented in the testbed can also be modified as a variety of schemes can be found in the literature, including those based on geographical and social targeting. Effectiveness of these approaches is substantially influenced by the compliance factor, for which limited accurate data support exists. It will thus be vital to gather the most detailed data on the epidemiology of a new virus and the population dynamics early in the evolution of a pandemic, and expeditiously analyze the data to adjust the interventions accordingly.

Future research. Future research efforts will focus on improving both model validity and its practical usability. We plan on increasing granularity of non-pharmaceutical interventions and implement *partial* school/workplace closure, such as closing individual classes or departments [30]. We will compare the societal and economic costs of such approaches to the costs of more conservative strategies of closing the entire institutions. To enable partial closure, the existing mixing groups will have to be partitioned into smaller subgroups. Another direction will include implementation of interventions based on social contact tracing [36]. Such approaches attempt to identify a certain number of social contacts of each infected individuals which can then be monitored and provided with prophylactic measures. If implemented at early pandemic stages, contact tracing may prove to be feasible and more resource efficient than “blanket" strategies. To improve model usability, we are working on developing an interface for (semi) automatic extraction of data from the following databases: demographical (U.S. Census Bureau [105] and Landscan [106]), social-behavioral (Consolidated Human Activity Database, CHAD [107]), travel (National Household Travel Survey, NHTS [92] and Eclipse-STEM [108]), and epidemiological surveillance (Early Aberration Reporting System, EARS, Enhanced Surveillance Project, ESP, and National Electronic Disease Surveillance System, NEDSS [109]).

To improve model scalability, we are working on enabling model execution in a distributed environment to perform time-stepped simulations of multiple simultaneous outbreaks. We are developing a tree/star computation structure [110–112], an environment in which starting with the root processor hosting a single-region, up to N processors may be required for an N-region pandemic. A time-stepped computation will evolve as a series of compute phases alternating with communication phases, as new processors (regions) join the computation. Such a structure will enable us to achieve the following advantages: (i) efficient partitioning of the data space across the processors, (ii) performing inter-processor message-exchange at the end of every time-step, and (iii) enabling efficient, data-streaming/-gathering to collapse data as it is routed up to the root for optimization control, parameter generation, and spread visualization. At the same time, we are also exploring replicate minimization techniques which alleviate computational burden without sacrificing statistical robustness of the model.

Acknowledgments

We would like to acknowledge with thanks the many helpful suggestions made by Prof. Yiliang Zhu, Department of Epidemiology and Biostatistics at the University of South Florida, Tampa, FL, USA.

Appendix. Supplementary data

Supplementary data associated with this article can be found in the online version, at doi:10.1016/j.seps.2011.05.001.

References

[1] World Health Organization (WHO). Cumulative number of confirmed human cases of Avian Influenza A(H5N1) reported to WHO, http://www.who.int/csr/disease/avian_influenza/country/cases_table_2010_08_31/en/index.html; 2010 [accessed 10.14.10].
[2] World Health Organization. Pandemic (H1N1) 2009-update 112, http://www.who.int/csr/don/2010_08_06/en/index.html; 2010 [accessed 10.14.10].
[3] Reuters. Swine flu can become drug-resistant quickly: study, http://www.reuters.com/article/idUSTRE68E5TZ20100915; 2010. Last accessed on 10/14/2010.
[4] Arthur Schoenstadt. Spanish flu, http://flu.emedtv.com/spanish-flu/spanish-flu.html; 2010 [accessed 10.14.10].
[5] Ungchusak K, Auewarakul P, Dowell SF, Kitphati R, Auwanit W, Puthavathana P, et al. Probable person-to-person transmission of avian influenza A (H5N1). New England Journal of Medicine 2005;352(4):333.
[6] Congressional Budget Office. A potential influenza pandemic: possible macroeconomic effects and policy issues, http://www.dhhs.state.nh.us/DHHS/CDCS/LIBRARY/Research/avian-cbo-economy.htm; 2008 [accessed 06.22.10].
[7] Fedson DS, Hant S. Pandemic influenza and the global vaccine supply. Clinical Infectious Deseases 2003;36:1552–61.
[8] Aunins JG, Lee AL, Volkin DB. Vaccine production. 2nd ed. Boca Raton: CRC Press LLC; 2000.
[9] World Health Organization. Pandemic (h1n1) 2009 vaccine deployment update – 17 december 2009, http://www.who.int/csr/disease/swineflu/vaccines/h1n1_vaccination_deployment_update_20091217.pdf; 2009.
[10] WHO Global Influenza Programme. Pandemic influenza preparedness and response. Technical report. World Health Organization; 2009.
[11] Poland GA. Vaccines against avian influenza – a race against time. New England Journal of Medicine 2006;354(13):1411–3.
[12] Christian MD, Hawryluck L, Wax RS, Cook T, Lazar NM, Herridge MS, et al. Development of a triage protocol for critical care during an influenza pandemic. Canadian Medical Association Journal 2006;175(11):1377.
[13] Oshitani H, Kamigaki T, Suzuki A. Major issues and challenges of influenza pandemic preparedness in developing countries. Emerging Infectious Diseases 2008;14(6):875.
[14] Centers for Disease Control and Prevention (CDC). Preparing for pandemic influenza, http://www.cdc.gov/flu/pandemic/preparedness.htm; 2007 [accessed 04.27.09].
[15] U.S. Department of Health & Human Services. HHS pandemic influenza plan, http://www.hhs.gov/pandemicflu/plan/; 2007 [accessed 03.27.09].
[16] Cauchemez S, Carrat F, Viboud C, Valleron A, Boelle P. A Bayesian (MCMC) approach to study transmission of influenza: application to household longitudinal data. Statistics in Medicine 2004;23:3469–87.
[17] Longini IM, Koopman JS. Household and community transmission parameters from final distributions of infections in households. Biometrics 1982;38:115–26.
[18] Longini M. The generalized discrete-time epidemic model with immunity: a synthesis. Mathematical Bioscience 1986;82:19–41.
[19] Yang Y, Halloran ME, Sugimoto J, Longini Jr IM. Detecting human-to-human transmission of avian influenza A (H5N1). Emerging Infectious Diseases 2007;13(9):1348–53.
[20] Ball F, Lyne O. Optimal vaccination policis for stochastic epdidemics among a population of households. Mathematical Biosciences 2002;177–178:333–54.
[21] Fraser C, Riley S, Anderson R, Ferguson N, May R. Factors that make an infectious disease outbreak controllable. PNAS 2004;101(16):6146–51.

[22] Carrat F, Lavenu A, Cauchemez S, Deleguer S. Repeated influenza vaccination of healthy children and adults:borrow now, pay later? Epidemiology and Infection 2005;134:63–70.
[23] Larson R. Simple models of influenza progression within a heterogeneous population. Operations Research 2007;55(399–412):165–95.
[24] Arino J, Brauer F, van den Driessche P, Watmough J, Wu J. Simple models for containment of a pandemic. Journal of Royal Society Interface 2006;3:453–7.
[25] Dargatz C, Georgescu V, Held L. Stochastic modelling of the spatial spread of influenza in germany. Austrian Journal of Statistics 2006;35(1):5–20.
[26] Ferguson N, Mallett S, Jackson H, Roberts N, Ward P. A population-dynamic model for evaluating the potential spread of drug-resistant influenza virus infections during community-based use of antivirals. Journal of Antimicrobial Chemotherapy 2003;51:977–90.
[27] Nigmatulina Karima R, Larson Richard C. Living with influenza: impacts of government imposed and voluntarily selected interventions. European Journal of Operational Research 2009;195(2):613–27. 6/1.
[28] Wu JT, Riley S, Fraser C, Leung G. Spatial considerations for the allocation of pre-pandemic influenza vaccination in the United States. Proceedings of the Royal Societyof London Biological Sciences 2006;274(1627):2811–7.
[29] Kelso JK, Milne GJ, Kelly H. Simulation suggests that rapid activation of social distancing can arrest epidemic development due to a novel strain of influenza. BMC Public Health 2009;9(1).
[30] Halder N, Kelso JK, Milne GJ. Analysis of the effectiveness of interventions used during the 2009 A/H1N1 influenza pandemic. BioMed Central 2010; 10(168).
[31] Yasuda H, Suzuki K. Measures against transmission of pandemic H1N1 influenza in Japan in 2009: simulation model. Euro surveillance: bulletin européen sur les maladies transmissibles = European Communicable Disease Bulletin 2009;14(44).
[32] Milne GJ, Kelso JK, Kelly HA, Huband ST, McVernon J. A small community model for the transmission of infectious diseases: comparison of school closure as an intervention in individual-based models of an influenza pandemic. PLoS One 2008;3(12).
[33] Longini IM, Halloran ME, Nizam A, Yang Y. Containing pandemic influenza with antiviral agents. American Journal of Epidemiology 2004;159(7): 623–33.
[34] Ferguson N, Cummings DA, Fraser C, Cajka J, Philip Cooley C, Burke DS. Strategies for mitigating an influenza pandemic. Nature 2006;442(27): 448–52.
[35] Das T, Savachkin A. A large scale simulation model for assessment of societal risk and development of dynamic mitigation strategies. IIE Transactions 2008;40(9):893–905.
[36] Ferguson NM, Cummings D, Cauchemez S, Fraser C, Riley S, Aronrag M, et al. Strategies for containing an emerging influenza pandemic in Southeast Asia. Nature 2005;437:209–14.
[37] Germann T, Kadau K, Longini IM, Macken C. Mitigation strategies for pandemic influenza in the United States. PNAS 2006;103:5935–40.
[38] Patel R, Longini I, Halloran M. Finding optimal vaccination strategies for pandemic influenza using genetic algorithms. Journal of Theoretical Biology 2005;234:201–12.
[39] Savachkin A, Uribe A, Das T, Prieto D. Developing dynamic predictive strategies for mitigation of cross-regional pandemic outbreaks. IIE Transactions (in review); 2010.
[40] Wu JT, Riley S, Fraser C, Leung G. Reducing the impact of the next influenza pandemic using household-based public health interventions. PLoS Medicine 2006b;3(9):1532–40.
[41] Glass R, Beyeler W, Min H. Targeted social distancing design for pandemic influenza. Emerging Infectious Diseases 2006;12(11):1671–81.
[42] Uribe, A., Prieto, D., Savachkin, A., Das, T., and Y. Zhu. A cross-regional pandemic outbreak simulation model: an aid to national resource allocation policy making. Proceedings of the 3rd INFORMS Workshop on Data Mining and Health Informatics (DM-DI 2008), 2008.
[43] Handel A, Longini I, Antia R. Towards a quantitative understanding of the within-host dynamics of influenza A infections. Epidemics 2009;1(3): 185–95.
[44] Pourbohloul B, Ahued A, Davoudi B, Meza R, Meyers LA, Skowronski DM, et al. Initial human transmission dynamics of the pandemic (H1N1) 2009 virus in North America. Influenza Other Respi Viruses 2009;3(5):215–22.
[45] Atkinson M, Wein L. Quantifying the routes of transmission for pandemic influenza. Bulletin of Mathematical Biology 2008;70(3):820–67.
[46] Pitzer VE, Olsen SJ, Bergstrom CT, Dowell SF, Lipsitch M. Little evidence for genetic susceptibility to influenza A (H5N1) from family clustering data. Emerging Infectious Diseases 2007a;13(7):1074–6.
[47] Pitzer VE, Leung GM, Lipsitch M. Estimating variability in the transmission of severe acute respiratory syndrome to household contacts in Hong Kong, China. American Journal of Epidemiology 2007b;166(3):355–9.
[48] Yang Y, Sugimoto JD, Halloran ME, Basta NE, Chao DL, Matrajt L, et al. The transmissibility and control of pandemic influenza A (H1N1) virus. Science 2009;326(5953):729–33.
[49] Colizza V, Barrat A, Barthelemy M, Vespignani A. The role of the airline transportation network in the prediction and predictability of global epidemics. PNAS 2006;103:2015–20.
[50] Epstein JM, Parker J, Cummings D, Hammond RA. Coupled contagion dynamics of fear and disease: mathematical and computational explorations. PLoS One 2008;3(12).
[51] Halloran ME. Invited commentary: challenges of using contact data to understand acute respiratory disease transmission. American Journal of Epidemiology 2006;164(10):945.
[52] Becker N, Starczak D. Optimal vaccination strategies for a community of households. Mathematical Biosciences 1997;139:117–32.
[53] Lee PY, Matchar DB, Clements DA, Huber J, Hamilton JD, Peterson ED. Economic analysis of influenza vaccination and antiviral treatment for healthy working adults. Annals of Internal Medicine 2002;137:225–31.
[54] Lipsitch M, Cohen T, Murray M, Levin BR. Antiviral resistance and the control of pandemic influenza. PLoS Medicine 2007;4(1):111–5.
[55] Miller G, Randolph S, Patterson JE. Responding to simulated pandemic influenza in San Antonio, Texas. Infection Control and Hospital Epidemiology 2008;29:320–6.
[56] Scharfstein DO, Halloran ME, Chu H, Daniels MJ. On estimation of vaccine efficacy using validation samples with selection bias. Biostatistics 2006;7(4): 615.
[57] Mills C, Robins J, Lipsitch M. Transmissibility of 1918 pandemic influenza. Nature 2004;432:904–6.
[58] Colizza V, Barrat A, Valleron A, Barthelemy M, Vespignani A. Modeling the worldwide spread of pandemic influenza: baseline case and containment interventions. PLOS Medicine 2007;4:95–110.
[59] Cooley P, Ganapathi L, Ghneim G, Holmberg S, Wheaton W, Hollingsworth C. Using influenza-like illness data to reconstruct an influenza outbreak. Mathematical and Computer Modelling 2008;48:929–39.
[60] Chao DL, Halloran ME, Obenchain VJ, Longini IM. FluTE, a publicly available stochastic influenza epidemic simulation model. PLoS Computational Biology 2010;6(1):e1000656.
[61] National Institute of General Medical Sciences. Models of infectious disease agent study, http://www.nigms.nih.gov/Initiatives/MIDAS/; 2008 [accessed 09.10.08].
[62] Longini IM, Nizam A, Shufu X, Ungchusak K, Hanshaoworakul W, Cummings D, et al. Containing pandemic influenza at the source. Science 2005;309:1083–7.
[63] Eubank S, Guclu H, Kumar V, Marathe M, Srinivasan A, Toroczkai Z. N.Wang. Modelling disease outbreaks in realistic urban social networks. Nature 2004; 429:180–4.
[64] Halloran ME, Ferguson NM, Eubank S, Longini I. Modeling targeted layered containment of an influenza pandemic in the United States. PNAS 2008; 105(12):4639–44.
[65] MIDAS. Report from the models of infectious disease agent study (MIDAS) steering committee, http://www.nigms.nih.gov/News/Reports/midas_steering_050404.htm; 2004 [accessed 09.10.08].
[66] Committee on Modeling Community Containment for Pandemic Influenza. Modeling community containment for pandemic influenza: a letter report, http://www.nap.edu/catalog/11800.html; 2006 [accessed 12.09.08].
[67] Centers for Disease Control and Prevention (CDC). Interim pre-pandemic planning guidance: community strategy for pandemic influenza mitigation in the United States, http://www.pandemicflu.gov/plan/community/community_mitigation.pdf; 2007 [accessed 04.01.09].
[68] Meltzer M, Cox N, Fukuda K. The economic impact of pandemic influenza in the United States: priorities for intervention. Emerging Infectious Deseases 1999;5(5):659–71.
[69] Savachkin A, Uribe-Sánchez A, Das T, Prieto D, Santana A, Martinez D. Supplemental data and model parameter values for cross-regional simulation-based optimization testbed, http://imse.eng.usf.edu/pandemic/supplement.pdf; 2010 [accessed 04.15.10].
[70] Lawless JF, Lawless JF. Statistical models and methods for lifetime data. New York: Wiley; 1982.
[71] Diekmann O, Heesterbeek JAP. Mathematical epidemiology of infectious diseases: model building, analysis and interpretation. Wiley; 2000.
[72] Brundage JF, Shanks GD. Deaths from bacterial pneumonia during 1918–19 influenza pandemic. Emerging Infectious Diseases 2008;14(8):1193.
[73] Centers for Disease Control and Prevention (CDC). CDC influenza operational plan, http://www.cdc.gov/flu/pandemic/cdcplan.htm; 2006 [accessed 03.27.09].
[74] World Health Organization (WHO). WHO guidelines on the use of vaccine and antivirals during influenza pandemics, http://www.who.int/csr/resources/publications/influenza/11_29_01_A.pdf; 2004. Retreived 03/27/2009.
[75] Pasteur S. Influenza A(H1N1) 2009 monovalent vaccine, http://www.fda.gov/downloads/biologicsbloodvaccines/vaccines/approvedproducts/ucm182404.pfd; 2009 [accessed 11.18.09].
[76] Blendon RJ, Koonin LM, Benson JM, Cetron MS, Pollard WE, Mitchell EW, et al. Public response to community mitigation measures for pandemic influenza. Emerging Infectious Diseases 2008;14(5):778.
[77] Sadique MZ, Edmunds WJ, Smith RD, Meerding WJ, de Zwart O, Brug J, et al. Precautionary behavior in response to perceived threat of pandemic influenza. Emerging Infectious Diseases 2007;13(9):1307.
[78] Maunder R, Hunter J, Vincent L, Bennett J, Peladeau N, Leszcz M, et al. The immediate psychological and occupational impact of the 2003 SARS outbreak in a teaching hospital. Canadian Medical Association Journal 2003; 168(10):1245–51.
[79] Robertson E, Hershenfield K, Grace SL, Stewart DE. The psychosocial effects of being quarantined following exposure to SARS: a qualitative study of Toronto health care workers. Canadian Journal of Psychiatry 2004;49:403–7.

[80] Pearson, M.L., Bridges, C.B., and S.A. Harper. Influenza vaccination of health-care personnel. Recommendations of the Healthcare Infection Control Practices Advisory Committee (HICPAC) and the Advisory Committee on Immunization Practices (ACIP)[Internet], 2006. [accessed 10.28.09].
[81] Keane M, Walter M, Patel B, Moorthy S, Stevens R, Bradley K, et al. Confidence in vaccination: a parent model. Vaccine 2005;23(19):2486–93.
[82] Niederhauser VP, Baruffi G, Heck R. Parental decision-making for the varicella vaccine. Journal of Pediatric Health Care 2001;15(5):236–43.
[83] Rhodes SD, Hergenrather KC. Exploring hepatitis B vaccination acceptance among young men who have sex with men: facilitators and barriers. Preventive Medicine 2002;35(2):128–34.
[84] Rosenthal SL, Kottenhahn RK, Biro FM, Succop PA. Hepatitis B vaccine acceptance among adolescents and their parents. Journal of Adolescent Health 1995;17(4):248–55.
[85] Smailbegovic M, Laing G, Bedford H. Why do parents decide against immunization? The effect of health beliefs and health professionals. Child: Care, Health & Development 2003;29(4):303.
[86] Colardo Department of Human Services Division of Mental Health. Pandemic influenza: quarantine, isolation and social distancing, http://www.flu.gov/news/colorado_toolbox.pdf; 2009 [accessed 10.28.09].
[87] Safranek TJ, Lawrence DN, Kuriand LT, Culver DH, Wiederholt WC, Hayner NS, et al. Reassessment of the association between Guillain-Barré syndrome and receipt of swine influenza vaccine in 1976–1977: results of a two-state study. American Journal of Epidemiology 1991; 133(9):940.
[88] Cummings KM, Jette AM, Brock BM, Haefner DP. Psychosocial determinants of immunization behavior in a swine influenza campaign. Medical Care 1979;17(6):639–49.
[89] The New Yorker. The fear factor, http://www.newyorker.com/talk/comment/2009/10/12/091012taco_talk_specter; 2009 [accessed 10.28.09].
[90] The New York Times. Doctors swamped by swine flu vaccine fears, http://www.msnbc.msn.com/id/33179695/ns/health-swine_flu/; 2009 [accessed 10.28.09].
[91] U.S Census Bureau. 2001 American community survey, http://www.census.gov/prod/2001pubs/statab/sec01.pdf; 2000 [accessed 03.27.09].
[92] Bureau of transportation statistics. 2001 National household travel survey (NTHS), http://www.bts.gov/programs/national_household_travel_survey/; 2002 [accessed 12.09.08].
[93] Tampa International Airport: daily traffic volume data, http://www.tampaairport.com; 2010 [accessed 04.07.10].
[94] Miami International Airport: daily traffic volume data, http://www.miami-airport.com; 2010 [accessed 04.07.10].
[95] Jacksonville Aviation Authority: daily traffic volume data, http://www.jaa.aero/General/Default.aspx; 2010 [accessed 04.07.10].
[96] Tallahassee Regional Airport: daily traffic volume data, http://www.talgov.com/airport/index.cfm; 2010 [accessed 04.07.10].
[97] How thermal-imaging cameras spot flu fevers, http://www.msnbc.msn.com/id/30523865/; 2010 [accessed 03.07.10].
[98] Writing committee of the World Health Organization (WHO). Consultation on human influenza A/H5. Avian influenza A(H5N1) infection in humans. New England Journal of Medicine 2005;353(13):1374–85.
[99] Institute of Medicine (IOM). Antivirals for pandemic influenza: guidance on developing a distribution and dispensing program. The National Academies Press; 2008.
[100] Treanor J, Campbell J, Zangwill K, Rowe T, Wolff M. Safety and immunogenicity of an inactivated subvirion influenza A(H5N1) vaccine. New England Journal of Medicine 2006;3554(13):1343.
[101] Blendon RJ, DesRoches CM, Cetron MS, Benson JM, Meinhardt T, Pollard W. Attitudes toward the use of quarantine in a public health emergency in four countries. Health Affairs 2006;25(2):15–25.
[102] Montgomery D. Design and analysis of experiments. John Wiley & Sons; 2007.
[103] Halfhill T. Inflation calculator, http://www.halfhill.com/inflatation.html; 2009 [accessed 12.04.09].
[104] Bell DM, et al. Non-pharmaceutical interventions for pandemic influenza, national and community measures. Emerging Infectious Diseases 2006; 12(1):88.
[105] U.S. Census Bureau. 2001 American community survey, http://factfinder.census.gov/home/saff; 2011 [accessed 03.27.11].
[106] Oak Ridge National Laboratory. LandScan, http://www.ornl.gov/sci/landscan/index.html; 2011 [accessed on 03/27/2011.
[107] Environmental Protection Agency (EPA). Consolidated human activity database, http://www.epa.gov/chadnet1/; 2011 [accessed 03.27.11].
[108] The ECLIPSE Foundation. Open healthcare framework. STEM component, http://www.eclipse.org/ohf/components/stem/; 2011 [accessed 01.25.11].
[109] Centers for Disease Control and Prevention (CDC). Emergency preparedness and response, http://www.bt.cdc.gov/episurv/; 2011 [accessed 04.06.11].
[110] Nakanishi H, Rego V, Sunderam V. On the effectiveness of superconcurrent computations on heterogeneous networks. Journal of Parallel & Distributed Computing 1995;24(2):177–90. Gordon Bell Prize Paper.
[111] Knop F, Mascarenhas E, Rego V, Sunderam V. Concurrent and fail-safe replicated simulations on heterogeneous networks: an introduction to EcliPSe. Simulation, Practice & Theory 1995;3:121–46.
[112] Knop F, Rego V, Sunderam V. Fail-Safe Concurrency in the EcliPSe System. Concurrency, Practice & Experience 1996;8(4):283–312.